Supporting Information

Kruglik et al. 10.1073/pnas.0912938107

SI Text

Origin of the $\nu_{\text{Fe-His}}$ Stretching Enhancement. The intensity of the $\nu_{\text{Fe-His}}$ stretching resonantly excited with the Soret electronic absorption depends upon the out-of-plane position of the iron (1). First, it has been shown that the $\nu_{\text{Fe-His}}$ stretching is coupled to the Soret ($\pi \rightarrow \pi^*$) transition (2). The enhancement due to Soret excitation depends upon the mixing of the π porphyrin and $\sigma_{\text{Fe-His}}$ molecular orbitals (1). A greater out-of-plane displacement of the iron increases this mixing (1) and consequently increases the intensity of the $\nu_{\text{Fe-His}}$ stretching when probed in resonance with the Soret band.

Heme Doming and NO Affinity. The observation that NO rebinds to a domed heme is also related to NO affinity and can be compared to the behavior of CO, which does not rebind on the picosecond time scale to Mb, for which the intensity of the $\nu_{\text{Fe-His}}$ stretching is constant (3) due to out-of-plane position of heme iron after CO dissociation, and whose geminate rebinding experiences an enthalpic barrier that has been assigned to the necessity of motion of the iron toward the heme plane (4). Hypotheses were proposed to explain ligand discrimination and the several orders of magnitude difference in affinity among NO, O_2, and CO, and there obviously exists several parameters influencing the affinity (5). The binding rate k_{on} depends on the protein structure itself (energy barriers for access to heme due to side chains) and on the barrier for direct interaction of the diatomic with the iron (heme-ligand reactivity). A major determinant for this latter barrier, differencing NO and CO, is the ability of binding to a domed heme. Thus the ability of the unpaired electron of NO to interact with the d_z^2 orbital of the high spin ferrous iron, whatever its position with respect to the heme plane, is a key parameter of heme-NO reactivity in Mb, contrary to CO.

Materials and Methods ***Time-resolved Raman spectroscopy.*** The time-resolved Raman spectroscopy apparatus has 0.7-ps temporal resolution and 25-cm^{-1} spectral resolution. It is based on a femtosecond Ti:sapphire laser whose amplified pulses (810 nm; ~0.6 mJ; 50 fs; 1 kHz) feeds a system comprising an optical parametric generator and two noncollinear optical parametric amplifiers for simultaneous generation of the photodissociating and Raman probe pulses. An interferential filter (0.45 nm FWHM) determines the parameters of the probe pulse (435 nm; 25 nJ; 0.7 ps; 25-cm^{-1}). The broad band photolysis pulse (560–570 nm; 2 μJ; 100 fs) is delayed by a motorized stage. The spectra were recorded with a 90° light-collection geometry by means of a camera lens before the spectrometer equipped with a liquid nitrogen cooled CCD. The photodissociating and probe beams were collinearly superimposed by a dichroic mirror and entered from the bottom of the cylindrical spinning sample cell. For measuring simultaneously $\nu_{\text{Fe-His}}$ and ν_4 (150–1700 cm^{-1} range; Fig. 3 and Fig. S2) we have used a 600 groves/mm grating instead of 1,200 groves/mm for the low-frequency range alone.

As recorded, the raw TR^3 spectra contain contributions from both the liganded and photolyzed heme and from the background. The background (spectrum with the pump beam only) is first subtracted from raw data and the resultant spectrum is corrected for the instrument function, then normalized to the intensity of the 980 cm^{-1} stretch of sulfate in the buffer. The pure transient TR^3 spectrum of the photoproduct at a given time delay is then obtained by subtracting the time-dependent contribution of the ground-state species (spectrum at −5 ps) whose weighting factor $K(\Delta t)$ is optimized to suppress all the negative features in the difference:

$$\text{product spectrum}(\Delta t) = \text{corrected spectrum}(\Delta t) - [K(\Delta t) \times \text{corrected spectrum}(-5\ \text{ps})].$$

Time-resolved absorption spectroscopy. Transient spectra were recorded simultaneously to kinetics as a time-wavelength matrix data using the pump-probe laser system previously described (6). Photodissociation of NO was achieved by excitation in the Q bands of the heme (wavelength 564 nm; pulse duration ~40 fs; repetition rate 30 Hz). The entire transient absorption spectrum after a variable delay between dissociating and probe pulses was recorded with a CCD detector. The global analysis of the data was performed by singular value decomposition (SVD) of the time-wavelength matrix as described (7). The SVD component having the highest singular value corresponded to the geminate rebinding and its kinetics were fit to a minimum number of exponential components (Table 1). The absorption kinetics (Fig. S1) are not at a single wavelength but are kinetics of a difference spectrum, taking into account the information from both the five-coordinate deoxy species decay and appearance of the six-coordinate liganded species.

Calculation of time-constant τ_D from the kinetics of $\nu_{\text{Fe-His}}$ intensity. The TR^3 difference spectra at Δt = 1–200 ps shown in Figs. 1 *A* and *C* and 4 *A*, *C*, *E*, and *G* are those of pure photoinduced transient species and Raman intensity of the $\nu_{\text{Fe-His}}$ band comes from all species having a domed structure, the 5c-His and 6c-His-NO heme (species X, B and D in Fig. 2*A*). The rate of the transition [domed 5c-His] → [domed 6c-His-NO] is that of NO rebinding measured by electronic absorption (τ_1 in Table 1). In the following analysis, the statement that domed five- and domed six-coordinate hemes have similar Raman excitation profiles is implicit, still awaiting theoretical calculations.

To obtain the time constant τ_D for the transition from domed 6-c to planar 6-c heme (D → A, Fig. 2), we resolved the rate equations for population decay of all nonplanar heme species using Mathematica program (Wolfram Research); the solution was convoluted with Raman instrumental response function (0.7 ps). The kinetic model employed was similar to that of Ionascu et al. (4) in which we introduced the additional species domed 6c-heme (D):

The set of following rate equations was solved:

$$dA/dt = k_{DA}D(t) \qquad dD/dt = k_{BD}B(t) - k_{DA}D(t)$$
$$dB/dt = k_{XB}X(t) - k_{BD}B(t) \qquad dX/dt = -k_{XB}X(t) \qquad \textbf{[S1]}$$

with the total population $A(t) + D(t) + B(t) + X(t) + \text{const} = 1$. The only planar heme species is $A(t)$ so that the total nonplanar population is $1 - A(t) = D(t) + B(t) + X(t) + \text{const}$. The initial conditions are $A(0) = 0$, $D(0) = 0$, while $X(0)$ and $B(0)$ are the normalized amplitudes of rebinding phases (Table 1) that describe the populations immediately after NO photodissociation. The rate constants $k_{XB} = 1/\tau_2$ and $k_{BD} = 1/\tau_1$ were measured by transient absorption. The constant term (const) corresponds either to a long NO rebinding phase ($\tau_3 > 5$ ns) or to bimolecular rebinding of NO in solvent. $K_{DA} = 1/\tau_D$ is the value to be determined and was varied until the curve describing the evolution

of the nonplanar population $D(t) + B(t) + X(t) + \text{const}$ fits the kinetics of experimental points obtained from the normalized area of the $\nu_{\text{Fe-His}}$ Raman contour.

Sample preparation. Horse heart myoglobin and mitochondrial horse heart cytochrome *c* were purchased from Sigma Chemical. The H64V myoglobin mutant and dehaloperoxidase (DHP) were expressed as described (8, 9). Mb and DHP were prepared in phosphate buffer (pH 7.4) and Hb type A (Sigma) was prepared in triethanolamine (TEA) buffer, pH 7.4. Mb in 50% glycerol was prepared in a mixture of TEA buffer and purified glycerol (Sigma). For transient absorption measurements, the solution of ferric proteins (100 μL; 75 μM) was put in a 1-mm optical path length quartz cell sealed with a rubber stopper and degassed by means of four successive cycles of vacuum and purging with argon (Air Liquide, 99.999%). The heme iron was reduced by the addition of 10 μL of degassed sodium dithionite ($Na_2S_2O_4$) or DTT to obtain 2-mM final concentration. For preparing the NO-liganded proteins [except cytochrome *c* (Cyt *c*)], gas phase 1% NO diluted in N_2 was directly introduced into the sample cell after vacuuming. Equilibrium spectra were recorded at each step for monitoring reduction and nitrosylation. The absorbance of the sample was in the range 0.6 to 0.8 at the Soret maximum for 1-mm path-length. For transient absorption Band III measurement, we used [Mb] = 4 mM (because absorption coefficient at 760 nm is only 100–120 $M^{-1} \cdot cm^{-1}$), and we reduced Mb with DTT at 10 mM. Then NO 10% was added.

Cyt *c* was dissolved in 0.1 M Tris/HCl buffer pH 7.4 and further purified by gel filtration in a Sephadex G-25 column (10 mL) connected to an Akta Purifier (Amersham Biosciences) using an isocratic elution with the same buffer. The chromatogramm monitored at 410 nm shows a main peak, which was collected, and a trailing edge which was discarded. The peak fraction was concentrated by ultrafiltration with a 5-kDa cutoff membrane and the buffer was exchanged for Tris-HCl pH 6.8. Purified ferric Cyt *c* (100 μL; 75 μM) was put in a 1-mm optical pathlength quartz cell, degassed, and reduced by the addition of 10 μL of degassed sodium ascorbate (Fluka) to obtain 2 mM final concentration. Nitrosylated Cyt *c* was prepared by replacing the argon gas phase with 100% NO at ~1.3 bar, yielding ~2 mM of NO in the aqueous phase.

For TR^3 measurements, 50 to 150 μL of a buffered solution of ferric proteins at a concentration of 0.3 mM (both 0.3 mM and 0.1 mM for wild type horse heart Mb) were placed in a cylindrical UV-quartz spinning cell (Hellma, Ref 540-135) sealed by a rubber stopper, vacuumed, and purged with argon. The OD was about 1 in the Q bands for an optical path length of 1 cm. The reduction of the proteins was performed as for absorption measurements. Then argon was replaced with NO 1% for Mb, Hb, and DHP and with NO 100% for Cyt *c*. All measurements were performed at 20 °C. For Mb in glycerol, we used 50% and not 80% glycerol because a too high viscosity of the sample resulted in the increased Rayleigh scattering background detrimental to the quality of TR^3 spectra.

1. Stavrov SS (1993) The effect of iron displacement out of the porphyrin plane on the resonance Raman spectra of heme-proteins and iron porphyrins. *Biophys. J.* 65:1942–1950.
2. Bangcharoenpaurpong O, Schomaker KT, Champion PM (1984) A resonance Raman investigation of myoglobin and hemoglobin. *J. Am. Chem. Soc.* 106:5688–5698.
3. Mizutani Y, Kitagawa T (2001) Ultrafast structural relaxation of myoglobin following photodissociation of carbon monoxide probed by time-resolved resonance Raman spectroscopy. *J. Phys. Chem. B* 105:10992–10999.
4. Ionascu D, et al. (2005) Temperature-dependent studies of NO recombination to heme and heme proteins. *J. Am. Chem. Soc.* 127:16921–16934.
5. Olson JS, Phillips GN (1997) Myoglobin discriminates between O_2, NO, and CO by electrostatic interactions with the bound ligand. *J. Biol. Inorg. Chem.* 2:544–552.
6. Martin JL, Vos MH (1992) Femtosecond biology. *Annu. Rev. Biophys. Biomol. Struct.* 21:199–222.
7. Negrerie M, Cianetti S, Vos MH, Martin JL, Kruglik SG (2006) Photoinduced coordination dynamics of cytochrome *c*: ferrous versus ferric species studied by time-resolved resonance Raman and transient absorption spectroscopies. *J. Phys. Chem. B.* 110:12766–12781.
8. Franzen S, et al. (2006) Hydrophobic distal pocket affects NO-heme geminate recombination dynamics in dehaloperoxidase and H64V myoglobin. *J. Phys. Chem. B* 110:14483–14493.
9. Li TS, Quillin ML, Phillips GN, Olson JS (1994) Structural determinants of the stretching frequency of CO bound to myoglobin. *Biochemistry* 33:1433–1446.
10. Lim M, Jackson TA, Anfinrud PA (1993) Nonexponential protein relaxation: dynamics of conformational change in myoglobin. *Proc. Natl. Acad. Sci. U.S.A.* 90:5801–5804.
11. Stavrov S.S. (2001) Optical absorption band III of deoxyheme proteins as a probe of their structure and dynamics. *Chem. Phys.* 271:145–154.

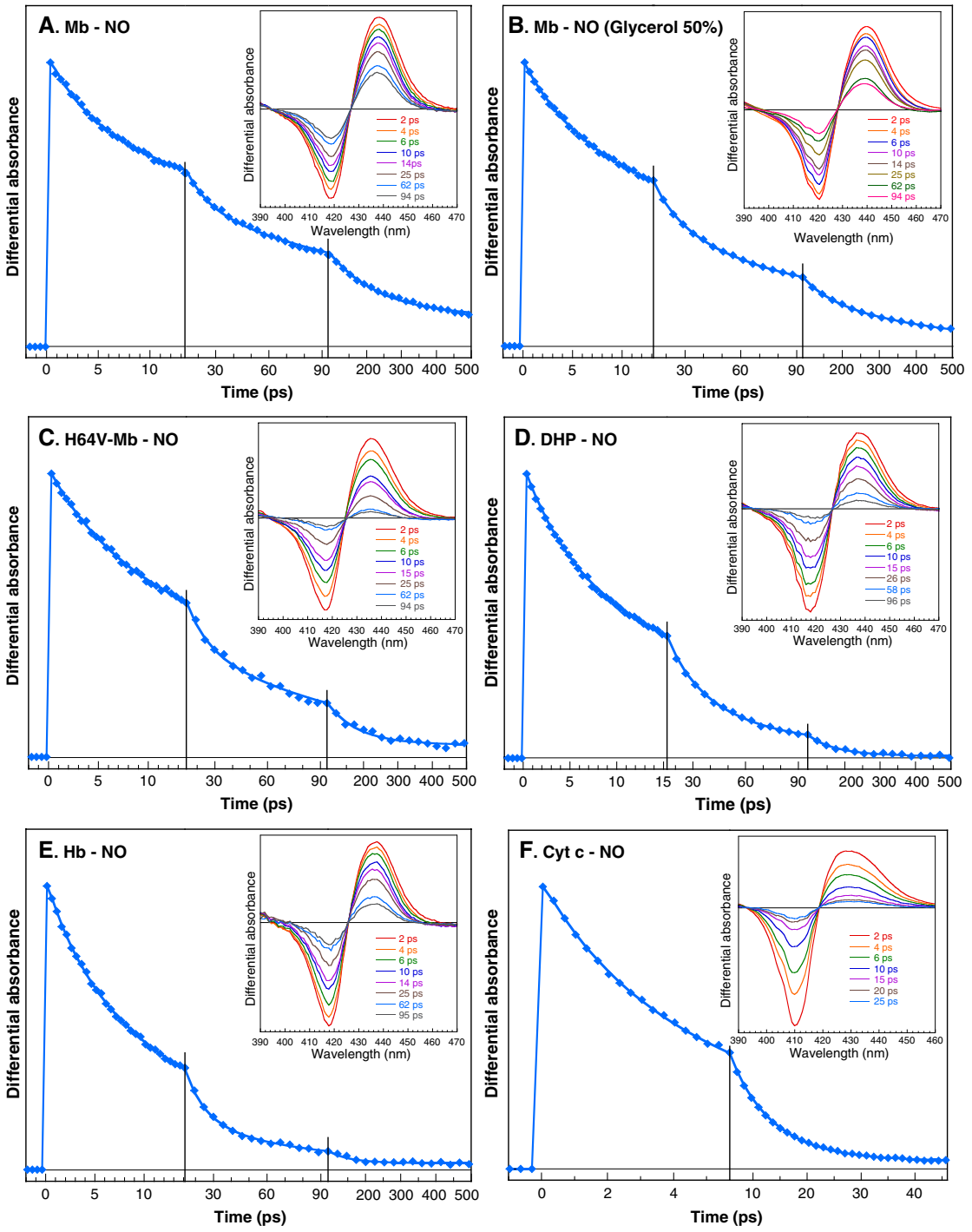

Fig. S1. Kinetics of NO rebinding from SVD analysis of the entire time-wavelength matrix and raw transient spectra (inserts) at different time delays. (*A*) myoglobin in water. (*B*) myoglobin in 50% glycerol. (*C*) H64V distal myoglobin mutant. (*D*) dehaloperoxydase. (*E*) hemoglobin. (*F*) mitochondrial cytochrome *c*. The corresponding parameters of the multiexponential fits of kinetics (solid lines through the data points) are displayed in Table 1.

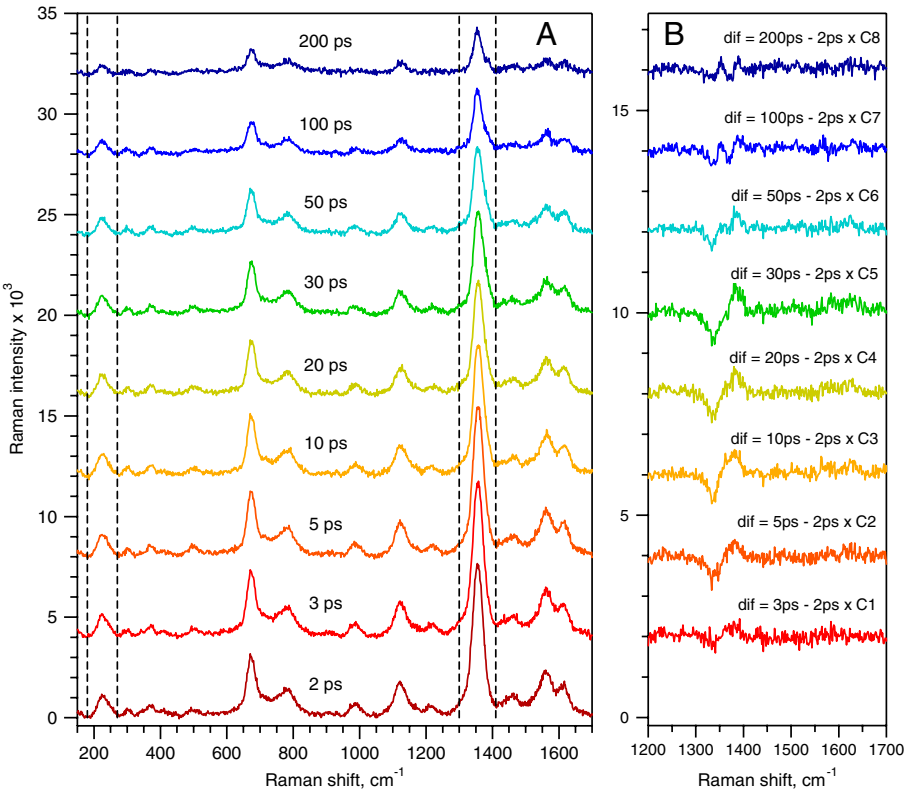

Fig. S2. Panel *A*: TR^3 spectra of Mb-NO photoproduct (species D + B + X + Const) after subtraction of the ground-state contribution, at indicated time delays (2 to 200 ps) between photolysis and Raman probe pulses. Vertical dashed lines indicate areas for $I_{Fe\text{-}His}$ (180–270 cm^{-1}) and I_{ν_4} (1300–1410 cm^{-1}) presented as markers in Fig. S3. Panel *B*: spectral difference in the high-frequency region of the ν_4-mode obtained by a weighted subtraction of the photoproduct Raman spectrum at 2 ps from photoproduct spectra at other time delays indicated above each trace. The values of subtraction coefficient are: C1 = 1, C2 = 1, C3 = 0.84, C4 = 0.74, C5 = 0.7, C6 = 0.55, C7 = 0.4, C8 = 0.26. The difference traces are not normalized.

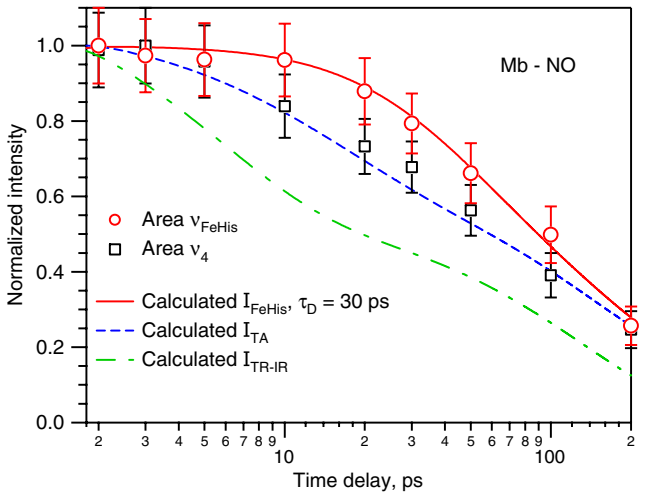

Fig. S3. Evolution of the normalized area under the $\nu_{Fe\text{-}His}$ (180–270 cm^{-1}, circles) and ν_4 (1300–1410 cm^{-1}, squares) Raman contours, corresponding to the experiment on Mb-NO presented in Figs. 3 and S2. Red, blue and green calculated curves are the same as in Fig. 1.

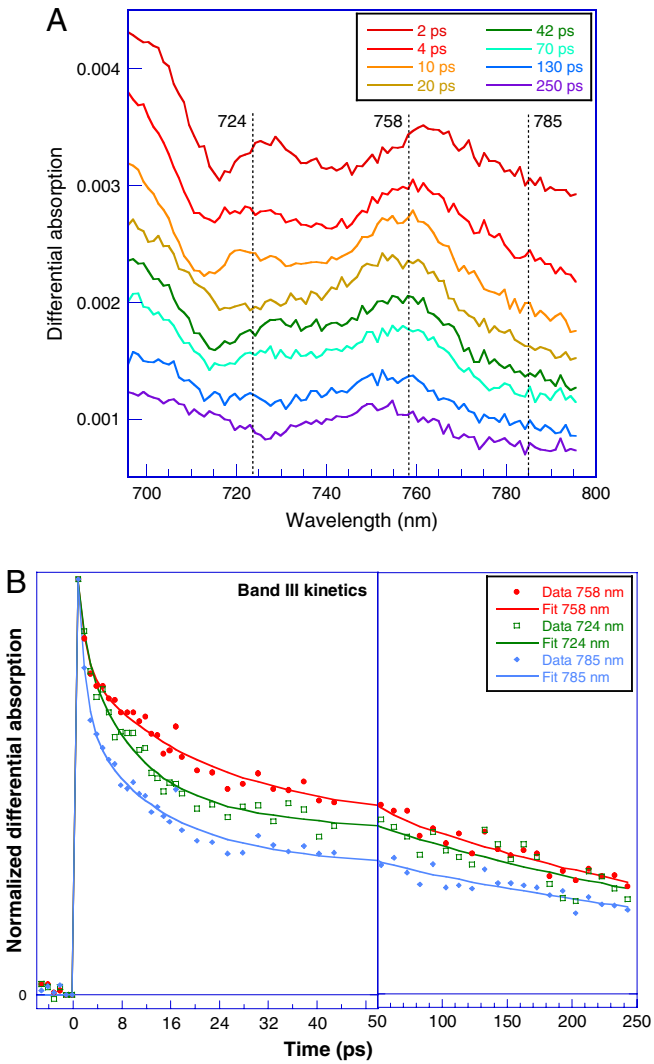

Fig. S4. Kinetics of the absorption Band III (755–760 nm, charge transfer transition) after Mb-NO photolysis, recorded with the same apparatus as the Soret absorption kinetics. Panel *A* : raw transient spectra at selected time delays. Spectra were not offset with respect to each other. Panel *B*: normalized kinetics at selected wavelengths, indicated by the dotted lines in panel A (raw kinetics, except normalization). The absorption coefficient of Band III is only 100–120 $M^{-1} \cdot cm^{-1}$, so that the amplitude of the broad underlying signal (10) is similar to that of Band III. The amplitude at 250 ps contains a contribution from bimolecular rebinding larger than that in Soret measurement due to the high Mb concentration (4 mM) compared to NO (2 mM). The main observation is that the kinetics at band III maximum is slower than that of the background (tail of the Q bands) comprising a slower phase from ~10 to 50 ps. Indeed, based on theoretical calculations, Band III intensity has been hypothesized to depend upon the Fe position with respect to the heme plane (11).